Applied Catalysis B: Environmental 237 (2018) 473–481

Contents lists available at ScienceDirect

Applied Catalysis B: Environmental

journal homepage: www.elsevier.com/locate/apcatb

Construction of a bifunctional electrode interface for efficient electrochemical mineralization of recalcitrant pollutants

Shouning Chai[a,b], Yujing Wang[c], Ya-nan Zhang[a], Hongying Zhao[a], Meichuan Liu[a], Guohua Zhao[a,*]

[a] School of Chemical Science and Engineering, Shanghai Key Lab of Chemical Assessment and Sustainability, Tongji University, Shanghai, 200092, China
[b] College of Science, Xi'an University of Architecture and Technology, Xi'an, Shaanxi, 710055, China
[c] School of Materials Science and Chemical Engineering, Xi'an Technological University, Xi'an, Shaanxi, 710032, China

ARTICLE INFO

Keywords:
Macroporous film
Electrocatalytic degradation
Colloidal crystal
Clofibric acid

ABSTRACT

To further improve the electrochemical performance of a boron-doped diamond (BDD) electrode, a two-dimensional, macroporous, Sb-doped SnO_2 film is constructed on BDD to obtain a bifunctional electrode interface (denoted Mp-SnO_2/BDD) with an ordered, monolayer, photonic-crystal template using a sol-gel method. SEM images confirm that the SnO_2 film consisted of innumerable, uniform, nanosized SnO_2 particles and numerous macropores with diameters of 200–300 nm, and some BDD polycrystallites are exposed in those macropores. The microstructure endows Mp-SnO_2/BDD with a high oxygen evolution potential (2.23 V), good conductivity (175 O), and excellent electrocatalytic activity. To evaluate the degradation capability, the electrocatalytic oxidation of a high concentration of clofibric acid (CA) is studied in detail. The CA and chemical oxygen demand (COD) removals on Mp-SnO_2/BDD are above 90% after 240 min. The degradation rate constant on Mp-SnO_2/BDD is 1.6 times that on BDD. Compared with BDD and traditional SnO_2/Ti, Mp-SnO_2/BDD exhibites a higher instantaneous current efficiency and lower electrochemical energy consumption. In addition, we qualitatively and quantitatively analyze the intermediates in the degradation process and proposed three possible oxidative decomposition pathways for CA. Mp-SnO_2/BDD is expected to be a promising anode for organic wastewater treatment.

1. Introduction

Electrochemical oxidation processes have attracted more attention for wastewater purification applications in recent years, and these processes are versatile approaches to degrade bio-refractory and toxic organic substances such as pesticides, pharmaceuticals, organic synthetic dyes, personal care products, and sanitary landfill leachate [1–4]. The electrode material is crucial for the optimization of electrochemical oxidation processes since it directly determines the oxidation efficiency, reaction mechanism and mineralization degree [5,6]. A new carbonaceous material, a polycrystalline boron-doped diamond (BDD) film, is widely considered an outstanding electrode because of its remarkable chemical inertness, good electrochemical stability, wide potential window, high mechanical strength, and poisoning resistance [7–9]. However, the low electrocatalytic activity and large electrical resistivity of BDD have severely hindered its further development for practical applications because they require long treatment periods and high energy consumption.

To overcome these drawbacks, BDD modification is a research hotspot in the field of electrocatalysis. For example, Comninellis et al. [10,11] and Yoshihara et al. improved the electrocatalytic redox activity by modifying the BDD surface with highly active Au particles/clusters [12]. Tong et al. constructed 3D, porous, vertical Pt nanosheets on BDD using a double template method, and the modified BDD showed a higher catalytic activity and better resistance to poisoning than BDD and Pt foil during a methanol electro-oxidation due to the larger electrochemical active area of porous Pt and the inherent poisoning resistance of BDD [13]. Although precious metals with different morphologies have a high electrocatalytic activity, their oxygen evolution potential (OEP) is relatively low in aqueous solutions. Thus, the OEP of BDD-based hybrid electrodes with precious metals will be reduced. This is unfavorable for the electrocatalytic oxidation of pollutants because a low OEP results in more side reactions during the oxygen evolution reaction and a decreased current efficiency. Additionally, the high cost of precious metals also severely limits the widespread utilization and commercial promotion of precious metal-

* Corresponding author.
E-mail address: g.zhao@tongji.edu.cn (G. Zhao).

https://doi.org/10.1016/j.apcatb.2018.06.023
Received 17 January 2018; Received in revised form 29 May 2018; Accepted 8 June 2018
Available online 15 June 2018
0926-3373/ © 2018 Elsevier B.V. All rights reserved.

modified BDD electrodes. Therefore, obtaining an anode with both a high OEP and outstanding electrocatalytic activity is important. We searched for an inexpensive metal oxide catalyst with a good electrocatalytic activity. Numerous studies have shown that Sb-doped SnO_2 (SnO_2) is an excellent electrocatalyst for organic pollutant removal, and it is especially suitable for complete mineralization of various recalcitrant carboxylic acids, phenols, perfluorocarboxylic acids, and halogenated aromatic compounds [14–16]. Sb-doped SnO_2 always exhibits a higher current efficiency than Pt, IrO_2, and RuO_2 electrodes, and this is attributed to its good conductivity and the rapid decomposition of intermediates on its surface [17–19]. In addition, SnO_2 has a relatively high OEP (1.9 V vs. SHE) [20,21]. Considering these characteristics, if modifying BDD with SnO_2 in a ingenious microstructure design will maintain the intrinsic OEP of BDD and substantially improve the electrocatalytic activity, which is undoubtedly a remarkable progress for advanced oxidation technology.

Herein, the focus was on creating a SnO_2-layer construction on a BDD surface. Obviously, the BDD surface can be easily covered by SnO_2 species with traditional methods such as spin-coating or doctor-blading. However, the hybrid electrode obtained would mainly exhibit the properties of SnO_2, and the inherent advantages of BDD would be lost because of a lack of exposure of the BDD surface. Therefore, we assumed that a two-dimensional, macroporous SnO_2 layer can be facilely constructed on BDD using a single-layer, hard template-assisted, dip-coating method to guarantee that SnO_2 and BDD are simultaneously exposed for the joint electrocatalytic oxidation. Over the past decade, a developed colloidal crystal-templated technique has been widely used for the preparation of various types of inorganic films with two- and three-dimensional, ordered macropores in the fields of optics, electronics, and energy [22,23], and this method provides a reliable reference to prepare macroporous SnO_2 layer.

In this work, a novel, bifunctional electrode interface of coexisting SnO_2 and BDD (Mp-SnO_2/BDD) was fabricated using monolayer colloidal crystal as a hard template. The morphology, physicochemical properties, and electrochemical performance of the as-prepared electrode were characterized. To evaluate the electrocatalytic activity and mineralization capability of the electrode, clofibric acid (CA) was selected as a toxic, bio-refractory, model organic pollutant for the electrochemical degradation. CA is an active ingredient and metabolite of clofibrate and other lipid regulators, and it is estimated to cause endocrine disruption and persist for over 20 years in the environment [24]. Many studies have reported the detection of CA in urban sewage, surface water and drinking water because it cannot be completely removed by traditional biological treatments [25,26]. The degradation efficiency, energy consumption, kinetics, and intermediates of the Mp-SnO_2/BDD electrode were determined. A possible CA mineralization mechanism was proposed. This research provides a new method for constructing new electrode materials, which is of great significance for electrocatalytic oxidation applications.

2. Experimental section

2.1. Materials

BDD (10 × 60 mm) was purchased from the Centre Suisse d'Electronique et de Microtechnique SA (CSEM, Switzerland) and was synthesized on a single-crystal p-Si (100) wafer using a microwave-assisted chemical vapor deposition technique. The final boron content was approximately 8000 ppm, and the average resistivity was ~0.1 Ω cm. A suspension of monodispersed polystyrene latex spheres (ac. 500 nm, 1 wt% in water) was purchased from Shenzhen Nanomicro Tech., China.

Methanol formic acid 4-chlorophenol, *p*-benzoquinone, maleic acid, and oxalic acid were HPLC grade, and $SnCl_2{\cdot}2H_2O$, $SbCl_3$, $(NH_4)_2HPO_4$, H_3PO_4 and CA et al. were analytical grade. All were purchased from Sigma-Aldrich Corporation, China (Mainland). HCl, H_2SO_4, and Na_2SO_4 were obtained from Sinopharm (Shanghai, China). All these chemicals were used as received without further purification. For solution preparation and chromatographic purposes, ultrapure water (Milli-Q water, Millipore) was used.

2.2. Fabrication of Mp-SnO_2/BDD

BDD was first treated in boiling aqua regia for 30 min to completely clean it. Then, BDD underwent anodic treatment at +3 V in 2 M H_2SO_4 for 30 min to obtain a −OH-terminated surface, and the BDD was finally ultrasonically washed with water, ethanol and water sequentially [27]. Based on the two-dimensional, self-assembly technique of colloidal microspheres in a wedge-shaped cell reported by the Wang group [28], monolayer polystyrene colloidal crystal was successfully assembled on the BDD surface. The colloidal crystal was used as a hard template, and they were combined with a sol–gel technique to prepare the Mp-SnO_2/BDD.

Before using, the colloidal suspension of polystyrene microspheres was diluted to 0.5 wt% with deionized water and sonicated for 30 min to disperse evenly. Two pieces of glass slides (1.0 cm × 10.0 cm) were served as substrates, which were immersed in a piranha solution at 90 °C for 30 min in order to create a hydrophilic surface and then rinsed with deionized water. Detailed procedures are as follows, two slides were clamped with a clip at one ends, and BDD as a wedge was placed in the middle of the two slides to form a wedge-shaped miniature cell with three opening sides. The angle between BDD and upper slides was adjusted to less than 5°, and then place the entire system horizontally. The cell was held horizontally and kept at ambient temperature (20–30 °C) with a relative humidity of 40% for 5–10 h after a small volume (50–100 μL) of colloidal suspension was injected into it. The suspension was immediately sucked into entire wedge space and spread evenly over the BDD surface owing to capillary force. Along with water evaporation, monolayer sphere arrays were crystallized via convective assemblies and showed a colorful appearance. Finally, a 2D colloidal crystal film grew onto BDD.

As the precursor solution, 10 g $SnCl_2{\cdot}2H_2O$ and 0.5 g $SbCl_3$ were dissolved in 100 mL ethanol that containing 10 mL concentrated hydrochloric acid. The mixed solution was stirred magnetically for 24 h to make it clear and saved stationarily for 12 h at room temperature. The as-prepared SnO_2 precursor sol was dip-coated (2 mm s^{-1}) vertically on the BDD assembled with 2D colloidal crystal. The sample was aged subsequently at 95 °C for 12 h and calcined at 450 °C for 1 h in air, then cooled to room temperature naturally. A Mp-SnO_2/BDD composite electrode was obtained. In addition, a contrastive SnO_2/Ti electrode in our study was also prepared by similar dip-coating procedure on a titanium sheet without 2D colloidal crystal as template.

2.3. Characterizations and electrochemical tests

The morphology of the electrode samples was characterized by scanning electron microscopy (FEG-SEM, Quanta 200 FEG, FEI), and their crystalline structure was characterized by X-ray diffraction (XRD, D/max2550VB3 + /PC, Rigaku) using a diffractometer with Cu Kα radiation, an accelerating voltage of 40 kV and a current of 40 mA. The elemental analyses of the electrode samples were performed using an X-ray photoelectron spectrometer (Axis Ultra DLD, Shimadzu, Japan) with monochromatized Al Kα radiation (1486.6 eV). The binding energy measurements were corrected for charging effects using the C 1 s peak of the adventitious carbon (284.6 eV) as a reference. The static state contact angle of pure water on the electrode surface was determined by drop shape analysis system DSA100 (Krüss, Germany) at room temperature.

All electrochemical measurements were carried out in a three-electrode cell of a CHI 660c electrochemical workstation (CHI Co., USA). BDD, Mp-SnO_2/BDD and SnO_2/Ti were used as the working electrode with a working area of 4 cm^2; a saturated calomel electrode

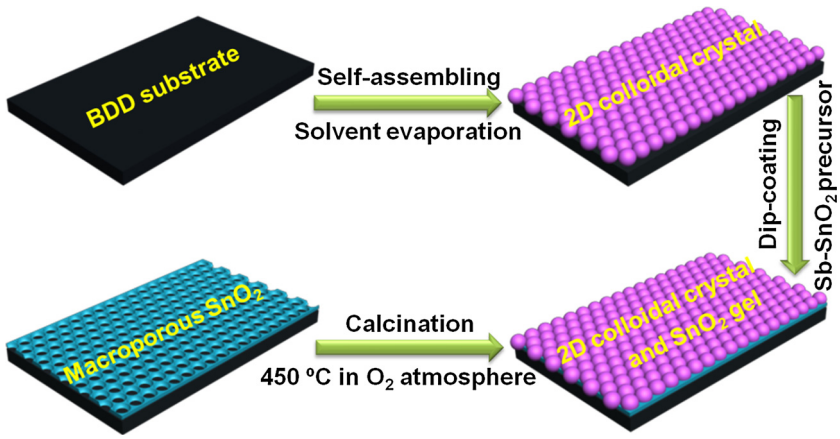

Scheme 1. Schematic illustration for the preparation of Mp-SnO_2/BDD.

(SCE) served as the reference electrode; Pt foil served as the counter electrode. The OEP was tested by the polarization curve method in a 1 M H_2SO_4 solution. Cyclic voltammetry (CV) was used to evaluate the electrocatalytic performance at a scan rate of 50 mV s^{-1}, and electrochemical impedance spectroscopy (EIS) was used to determine the conductivity of the anodes at the open circuit potential and an amplitude of 5 mV over a frequency range from 1×10^5 to 1×10^{-3} Hz in a 0.5 mM $[Fe(CN)_6]^{3-}/[Fe(CN)_6]^{4-}$ solution. In addition, the electrocatalytic oxidation capability for CA was determined by CV and the curve of the current density versus time (i–t) in a 0.05 M Na_2SO_4 solution containing 200 mg L^{-1} CA.

2.4. Degradation experiment and analysis of the degraded samples

The electrochemical degradation was carried out in a cylindrical, single-compartment cell equipped with a jacketed cooler to maintain a constant temperature (25 ± 2 °C). BDD, Mp-SnO_2/BDD and SnO_2/Ti were used as the anode with a working area of 4 cm^2, and a Pt sheet with the same area was used as the cathode with an electrode gap of 1 cm. A 100 mL simulated wastewater with 200 mg L^{-1} CA ($C_{10}H_{11}ClO_3$) in a 0.05 M Na_2SO_4 solution was degraded with magnetic stirring. The current density was held constant at 30 mA cm^{-2} by a direct-current potentiostat.

The concentrations of the CA and carboxylic acid intermediates during the degradation were measured by high-performance liquid chromatography (HPLC, Agilent HP1100) using an AQ-C18 column (4.6 mm × 250 mm, particle size 5 μm) and a UV detector at λ = 228 nm and 215 nm. All the samples were filtrated using disposable syringe filters (13 mm × 0.20 μm). Methanol/water mixtures (70:30 (v/v)) containing 0.2% formic acid and a 0.5% $(NH_4)_2HPO_4$-H_3PO_4 (pH = 2.4) solution were employed as the mobile phase for the CA and carboxylic acid intermediate detection with a flow rate of 1.0 mL min^{-1} at room temperature. The injection volume was 20 μL A gas chromatography-mass spectrometry (GC–MS) analysis was also performed to identify the main intermediate products that formed during the CA degradation process. The degradation samples were pretreated by liquid-liquid extraction with a CH_2Cl_2 solvent to extract and concentrate the compounds with different polarities and volatilities. The extracts were dried by anhydrous sodium sulfate overnight. The finished samples were concentrated to 1–2 mL under reduced pressure and then analyzed. The spectra were obtained using a gas chromatograph (Agilent 7890 A) equipped with a DB-5 MS capillary column (30 mm × 320 μm, 0.5 μm film thickness) directly interfaced to the mass spectrometer (5975 A inert XL MSD with Triple-Axis Detector) used as a detector. The GC column was operated in a temperature programmed mode with an initial temperature of 40 °C, which was held for 1 min, ramped to 240 °C at 10 °C min^{-1}, and held for 3 min. The injector temperature was 280 °C, and helium served as the carrier gas at a flow rate of 1 mL min^{-1}. The electron impact (EI) mode at 70 eV was used, and the scanned mass range was 10–400 *m/z*. The substance analysis was referenced to the NIST08 mass spectral library database.

The chemical oxygen demand (COD) was determined by the potassium dichromate method. Chloride ion selective electrode (BELL-Cl-, BELL Ananlytical Instruments Co., Ltd., China) was used to measure the chloride ion released from the CA degradation process. The instantaneous current efficiency (ICE) for the electrochemical oxidation of CA was calculated from the COD values using the following [29,30]:

$$\mathrm{ICE} = \frac{(\mathrm{COD}_t - \mathrm{COD}_{t+\Delta t}) \times F \times V}{8 I \Delta t} \quad (1)$$

where COD_t and $COD_{t+}\Delta_t$ (mg L^{-1}) are the COD values at electrolysis time t and t +Δt (s), respectively; *I* is the current (A); *F* is the Faraday constant (96,485 C mol^{-1}); *V* is the volume of the electrolyte (L); and 8 is the equivalent mass of oxygen.

The average electrical energy consumption (EC_{COD}) in kWh mg^{-1} of the COD was defined as the average amount of electrochemical oxidation energy required to remove 1 mg of COD [21,31],

$$\mathrm{EC_{COD}} = \frac{E_{\mathrm{cell}} \times I \times \Delta t}{(\mathrm{COD}_0 - \mathrm{COD}_t) \times V} \quad (2)$$

where E_{cell} is the potential difference of the cell (V), and the other symbols are the same as those previously mentioned.

3. Results and discussion

3.1. Formation, morphology and physicochemical properties of Mp-SnO_2/BDD

The schematic illustration for the Mp-SnO_2/BDD fabrication is depicted in Scheme 1. The Mp-SnO_2 was successfully assembled on the BDD substrate using a monolayer, polystyrene colloidal crystal template and a sol-gel method. The BDD was cleaned and pretreated via complete oxygen termination to ensure the surface was hydrophilic. As shown in Fig. 1A, the thin, polycrystalline film grown on a Si wafer is crack-free and consists of innumerable crystallite grains with micrometer-scale sizes [27]. The monodispersed polystyrene spheres self-assemble under capillary forces to form a two-dimensional (2D), colloidal crystal with long-range order on the BDD substrate. Fig. 1B shows that the diameter of the polystyrene spheres is uniform (~500 nm), and the single-domain, colloidal crystal has a hexagonal, close-packing structure, which is attributed to the balanced interparticle forces in a colloidal system. Then, a 2D colloidal crystal film was employed as the hard template, and a Sb-SnO_2 precursor solution permeated into the interspaces between the spheres during the dip-coating process. In the subsequent aging process, the sol slowly hydrolyzed and condensed into

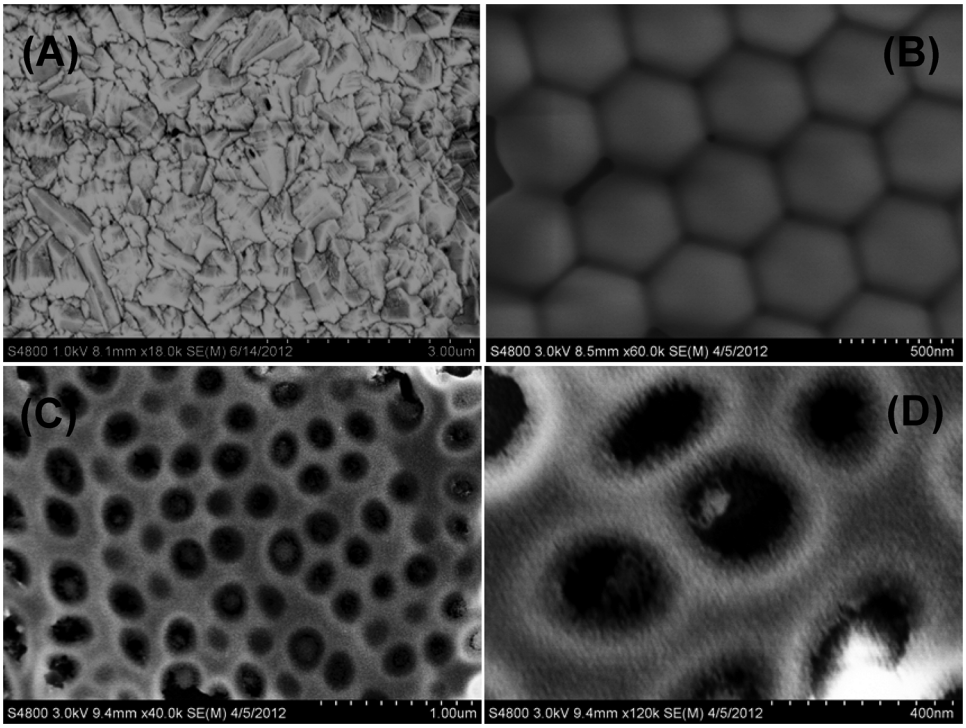

Fig. 1. SEM images of BDD (A), 2D colloidal crystal template on BDD (B), and Mp-SnO_2/BDD at low (C) and high (D) magnification.

a gel. Pyrolysis completely removed the polystyrene template, and the gel on the BDD decomposed into a single-layer, macroporous, Sb-doped, SnO_2 film containing numerous nanosized grains. Although the BDD surface is uneven on the nanoscale level, the distribution of the macropores is well-organized because of the ordered colloid crystal template. The pore diameter is 200–300 nm (Fig. 1C). Moreover, Fig. 1D shows that the BDD polycrystal is sufficiently exposed by the macropores, and the novel Mp-SnO_2/BDD electrode can simultaneously provide two interfaces, i.e. the Sb-doped SnO_2 electrocatalyst surface and the BDD substrate surface.

An XRD analysis was conducted to identify the phase composition of the electrodes (Fig. 2A). The XRD pattern of Mp-SnO_2/BDD has three peaks at $2\theta = 26.6°$, 33.9° and 53.0°, which can be referenced to the (110), (101), and (211) planes of the tetragonal rutile phase of SnO_2, and the diamond (111) and (220) plane diffraction peaks at 44.6° and 75.8°, respectively [32,33]. Sb doping is crucial for obtaining the excellent conductivity and electrochemical performance of the SnO_2 electrode, however, the diffraction peaks of Sb or SbO*x* were not observed due to the low doping content and the similar ionic radii of Sb^{5+} (78 pm) and Sn^{4+} cations (83 pm). In this case, Sb is easily doped into the SnO_2 lattice to form a good solid solution [34].

To confirm the valence states of the metal cations, the surface of the as-prepared Mp-SnO_2/BDD was characterized by XPS. The survey spectrum (Fig. S1) shows several strong peaks assigned to Sn 3p, O 1 s, Sn 3d, and C 1 s, indicating that the Mp-SnO_2/BDD surface is composed of tin oxide and diamond. In the Sn 3d region (Fig. 2B), the spectrum has two symmetry peaks at 486.7 eV (Sn $3d_{5/2}$) and 495.2 eV (Sn $3d_{3/2}$), and the peak interval is 8.5 eV, which agrees with the standard spectrum of SnO_2 [35,36]. Fig. 2C shows the high-resolution spectrum of Sb 3d, and the two peaks at 530.8 eV and 540.2 eV with a peak interval of 9.4 eV can be attributed to Sb $3d_{5/2}$ and Sb $3d_{3/2}$ in Sb_2O_5, respectively. According to previous literatures, the Sb $3d_{3/2}$ peak of Sb_2O_3 is generally located at a binding energy of 539.5–539.6 eV, indicating that the Sb doped in the SnO_2 film is mainly in the +5 valence state [35,36].

3.2. Enhanced electrochemical properties and activity

To study the electrochemical performance, EIS of the electrode can be used to determine the electron transfer resistance (R_{et}) at the electrode interface in solution. Fig. 3A shows the EIS results for Mp-SnO_2/BDD and BDD in a 5 mM $[Fe(CN)_6]^{3-}/[Fe(CN)_6]^{4-}$ solution. The Randles model equivalent circuit (Inset in Fig. 3A) was used to fit the impedance spectra. The fitted R_{et} value of Mp-SnO_2/BDD is 175 O, which is much lower than that of BDD (3850 O). The high R_{et} of BDD is attributed to the sp^3 hybrid structure of the carbon atoms in the diamond. The results show that assembling a SnO_2 layer with good electrical conductivity on BDD is beneficial for charge transfer. The 2D, macroporous structure facilitates the electron and mass transport, which are important for reducing the electrochemical impedance and enhancing the current efficiency. To investigate the electrocatalytic behavior of Mp-SnO_2/BDD, cyclic voltammograms were also measured in the same test solution. As illustrated in Fig. S2, the redox peak on BDD is small, and the current densities equal 0.79 mA cm^{-2} and −0.50 mA cm^{-2} due to the high electrochemical impedance and poor electrocatalytic activity. However, the corresponding peak values increase to 1.26 mA cm^{-2} and −1.14 mA cm^{-2} on Mp-SnO_2/BDD, which indicates that more substances are involved in the electrochemical redox reactions on Mp-SnO_2/BDD than those on BDD under the same conditions. The potential difference, ΔEp, between the anodic and cathodic peaks for Mp-SnO_2/BDD is 132 mV less than that for BDD, which indicates that the redox reaction of the $[Fe(CN)_6]^{3-}/[Fe(CN)_6]^{4-}$ redox couple requires less energy. Meanwhile, the cyclic voltammogram of Mp-SnO_2/BDD is more symmetrical than that of BDD, which indicates a better electrode reversibility. Therefore, the modification of SnO_2 is also beneficial for improving the electrocatalytic activity of BDD.

The OEP is another important parameter to evaluate the electrochemical performance of an anode material. BDD stands out among so many electrochemical anodes because of its high OEP. Nevertheless, the OEP of SnO_2 is generally lower than that of BDD, 1.7–1.8 V (vs. SCE). Fig. S3 shows the polarization curves of Mp-SnO_2/BDD and BDD in a 1 M H_2SO_4 solution. The OEP of the BDD electrode is 2.35 V (vs. SCE).

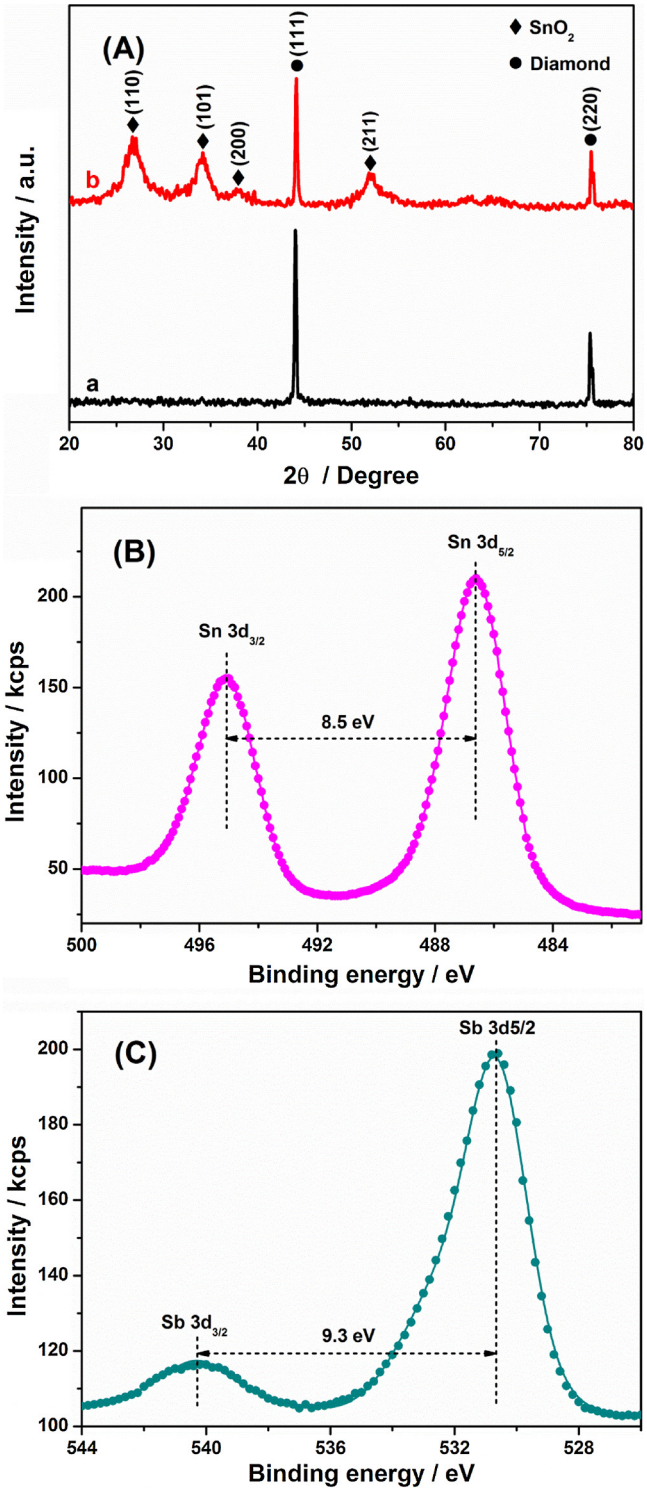

Fig. 2. (A) XRD patterns of BDD (a) and Mp-SnO_2/BDD (b); Sn 3d (B) and Sb 3d (C) XPS spectra of Mp-SnO_2/BDD.

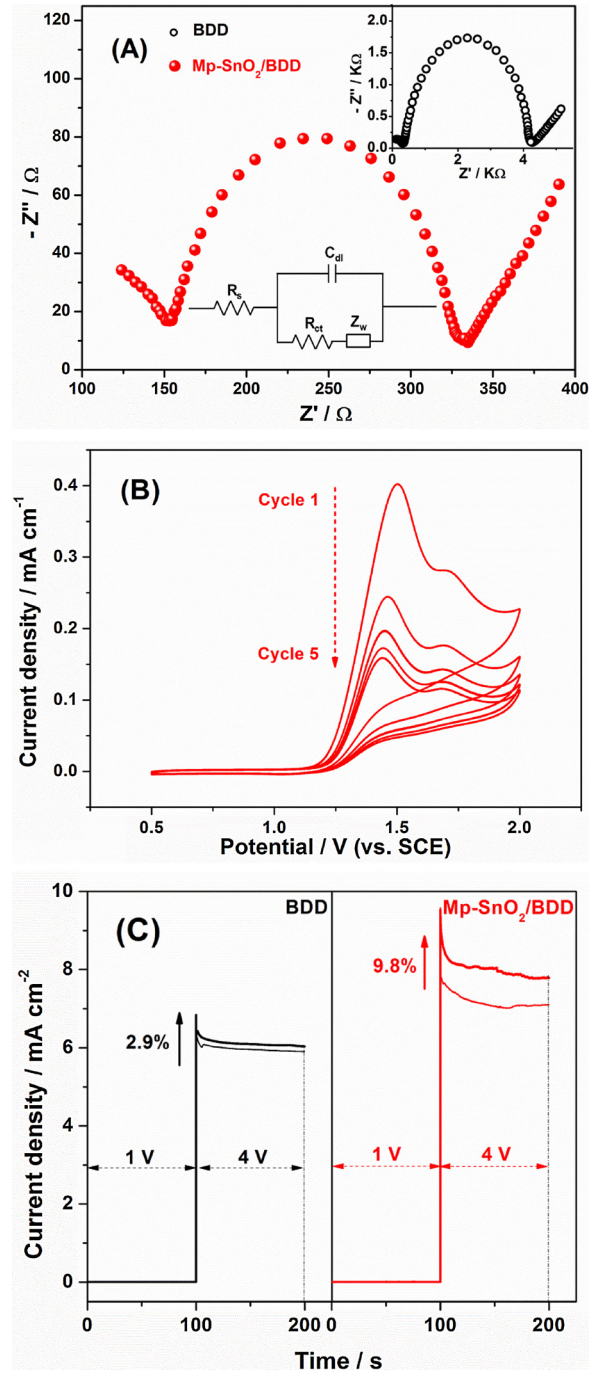

Fig. 3. (A) Nyquist plot of Mp-SnO_2/BDD in a 5 mM $[Fe(CN)_6]^{3-}/[Fe(CN)_6]^{4-}$ solution, inset: the corresponding equivalent circuit model and Nyquist plot of bare BDD in the same solution; (B) Cyclic voltammograms of Mp-SnO_2/BDD in a 0.05 M Na_2SO_4 + 200 mg L^{-1} CA solution at a scan rate of 50 mV s^{-1} for 5 cycles; (C) Changes of the current density over time for BDD and Mp-SnO_2/BDD in a 0.05 M Na_2SO_4 solution and 0.05 M Na_2SO_4 + 200 mg L^{-1} CA solution at 1 V and 4 V (vs. SCE), respectively.

After assembling the macroporous SnO_2 layer, some of the BDD surface is still exposed by the countless, sieve-like macropores, and thus, Mp-SnO_2/BDD still maintains a relatively high OEP of 2.23 V. The small decrease is probably related to the wettability change of the electrode. As is known, as-grown BDD via CVD is largely hydrogen terminated and hydrophobic in nature. To study the wettability, the static state contact angles of pure water on the electrodes surface were determined. Fig. S4 shows an optical image of a 5 μL pure water drop on the BDD and Mp-SnO_2/BDD. The contact angle is about 100° at BDD. After it was modified with hydrophilic macroporous SnO_2 film, the contact angle reduces to 45° and a distinct decrease of hydrophobicity is observed. Although the OEP of Mp-SnO_2/BDD is lower than that of pristine BDD but much higher than that of traditional, dimensionally stable SnO_2 anodes, ensuring that the electrode still exhibits a strong mineralization ability for recalcitrant organic pollutants. During anodnic electrochemical oxidation, a competition often exists between the main pollutant degradation reaction and the oxygen evolution side reactions. In

aqueous solutions, when a certain high voltage is applied to the anode, the H_2O molecules decompose on the anode interface to produce adsorbed/free ·OH, which may attack the surrounding pollutant molecules or combine to generate O_2. Therefore, if the OEP of an anode is low, i.e., lower than the oxidative decomposition potential of the dissolved organic pollutants, the ·OH ratio for the pollutant oxidation is limited, which results in a decrease in the current efficiency and an increase in the energy consumption [37]. The situation is the opposite for Mp-SnO_2/BDD; i.e., O_2 evolution is difficult, and the electrochemical mineralization efficiency is improved by the high chance of organic pollutants being oxidized by •OH. Mp-SnO_2/BDD maintains a high OEP, which implies that it has a high current efficiency and a low energy consumption during the electrochemical oxidation process.

3.3. Efficient electrochemical incineration of CA

To evaluate the electrochemical oxidation ability, Mp-SnO_2/BDD was used to degrade 200 mg L^{-1} of CA. Considering the environmental behavior and ecotoxicity of CA, studies on the electrochemical degradation of high levels of CA, it degradation intermediates, and degradation pathways are very important [38–41]. The CA concentration as a function of the degradation time is presented in Fig. 4A. After 240 min, the CA concentration decreases to 10 mg L^{-1} from an initial concentration of 200 mg L^{-1} with Mp-SnO_2/BDD, and the removal ratio of the target pollutant is 95%. In comparison, the degradation ratios of CA with BDD and SnO_2/Ti are 83% and 65%, respectively. The derived curve of $\ln(C_0/C)$ versus time shows a good linear relationship, illustrating the degradation reaction kinetics are pseudo-first-order kinetics (Inset of Fig. 4A). The apparent rate constant (k_{app}) value on Mp-SnO_2/BDD is 0.013 min^{-1}, which is 1.6 and 2.6 times greater than that on BDD and SnO_2/Ti, respectively. The degradation efficiency on Mp-SnO_2/BDD is the highest, and this electrode has the best electrocatalytic oxidation capability for organic pollutant decomposition. In general, the complete mineralization of recalcitrant pollutants is desired for wastewater treatment. Thus, monitoring the evolution of COD is necessary. As shown in Fig. S5, within 240 min, the COD removals are 90%, 75%, and 58% on Mp-SnO_2/BDD, BDD, and SnO_2/Ti, respectively. Obviously, Mp-SnO_2/BDD has the best electrocatalytic behavior for the original pollutant and exhibits a higher continuous oxidation ability for various intermediate products than the other two electrodes, which is consistent with the CV results in CA solutions; i.e., Mp-SnO_2/BDD has the strongest anti-fouling and anti-deactivation abilities. The ICE and EC at each stage of the degradation process were calculated according to Eqs. (1) and (2). As shown in Fig. 4 B, the ICE values all decreased over time for the three electrodes, but the ICE of Mp-SnO_2/BDD is higher than that of the other two electrodes at all times. The ICE of Mp-SnO_2/BDD reaches 43% in the initial stage (30 min), which is much higher than 28% for BDD and 14% for SnO_2/Ti. A higher current efficiency always results in a smaller energy consumption. For a COD removal rate of 30%, the EC is only 0.06 kW h mg^{-1} COD on Mp-SnO_2/BDD, but the EC is 0.12 kW h mg^{-1} COD and 0.15 kW h mg^{-1} COD on BDD and SnO_2/Ti, respectively, for the degradation. This is mainly attributed to three reasons. When the macroporous SnO_2 layer is constructed on the BDD, the conductivity is greatly improved, and the cell voltage required to maintain the same level of electrocatalytic degradation decrease. Second, the significant increase in the number of catalytic active sites endowes Mp-SnO_2/BDD with an excellent electrocatalytic oxidation capacity, ensuring the efficient COD decay. Third, the rapid generation of ·OH is also maintained because Mp-SnO_2/BDD has a high OEP, which was a prerequisite for the complete mineralization of organic pollutants.

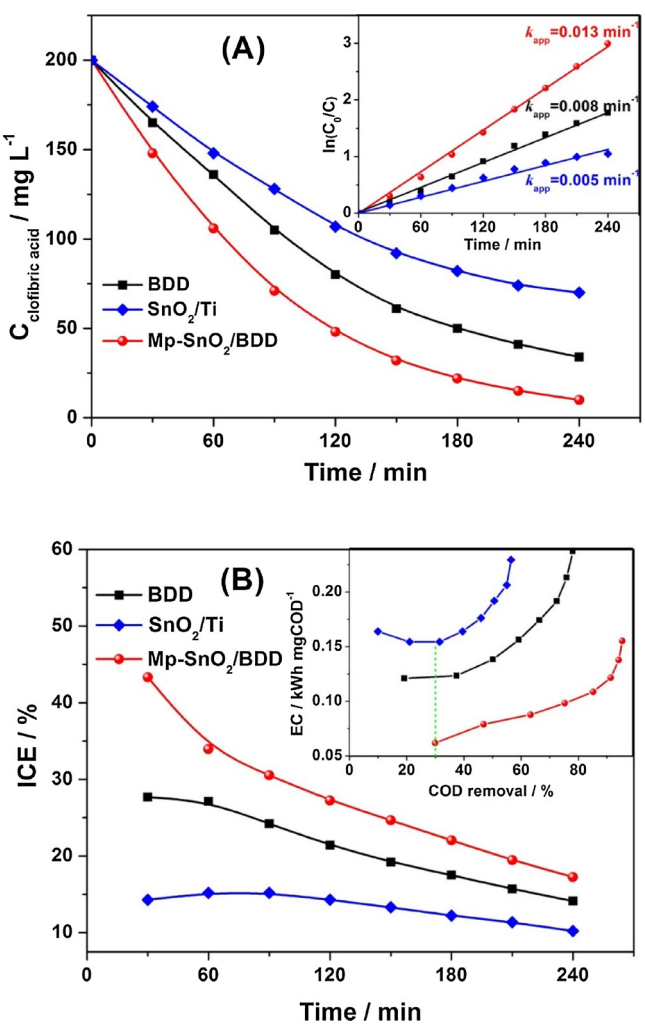

Fig. 4. CA removal (A) and instantaneous current efficiency changes (B) as a function of degradation time for the three different anodes; Insets of (A) and (B): The kinetics of CA degradation, and the changes in the average energy consumption as a function of the COD removal ratio.

3.4. Proposed degradation pathways and mechanism

Nine intermediates were identified by GC–MS and/or HPLC analyses during the electrochemical treatment of CA. Their chemical names, structures and main mass fragmentation data are summarized in Table S1. The aromatic intermediates detected by GC–MS were 4-chlorophenol, hydroquinone, 4-chlorocatechol, p-benzoquinone and 1,2,4-benzenetriol, and four carboxylic acids with short chains, maleic acid, fumaric acid, oxalic acid and formic acid, were detected by HPLC, which was consistent with the previous literature results [30,42]. Additionally, the evolution of four intermediates (4-chlorophenol, hydroquinone, maleic acid, and formic acid) was quantitatively determined by HPLC using standard substances to determine the degradation kinetics, as shown in Fig. 5. Generally, for organic pollutants containing benzene ring structures, various aromatic derivatives can be rapidly generated and accumulated because the large benzene ring is likely to be attacked by ·OH. A typical, parabola-like trend in the concentrations of the intermediates is observed on Mp-SnO_2/BDD and BDD (Fig. 5A, B); i.e., two main intermediates accumulate in the first stage due to the elementary decomposition of the parent molecules, and they are progressively converted into other by-products and/or CO_2 and H_2O after reaching a maximum concentration (c_{max}). However, the c_{max} values are different; c_{max} values of 5.0 and 2.4 mg L^{-1} are attained for 4-chlorophenol and hydroquinone, respectively, in solution samples treated with Mp-SnO_2/BDD, and the corresponding values are 6.9 and 3.8 mg L^{-1} with BDD, respectively. The low c_{max} values imply that Mp-SnO_2/BDD possesses a strong electrochemical oxidation capacity. In this case, the accumulation of toxic intermediates on the electrode

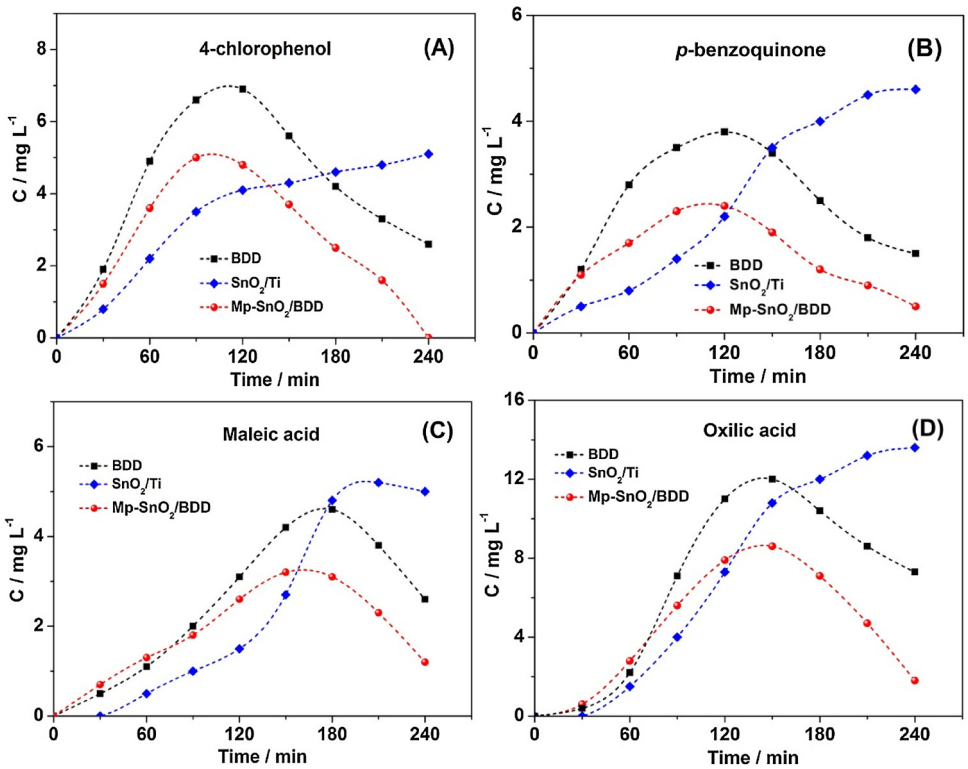

Fig. 5. The concentrations of intermediates as a function of time, (A) 4-chlorophenol, (B) *p*-benzoquinone, (C) maleic acid, and (D) oxalic acid during the electrocatalytic degradation of CA with three different electrodes.

interface is greatly reduced, which can effectively suppress the electrode deactivation caused by electro-polymerization and avoid a reduction in the current efficiency. Although SnO_2/Ti also has a good electrocatalytic activity, the yield of ·OH is not high because of its relatively low OEP. Therefore, the concentrations of 4-chlorophenol and benzoquinone continue to slowly increase, and a c_{max} value is not observed during degradation process. Fig. 5C, D depict the concentration changes of maleic acid and oxalic acid. Maleic acid is derived from a ring-opening reaction of the aromatic intermediates and is further oxidized to produce oxalic acid. Therefore, their c_{max} values occur at approximately 180 min. Throughout the degradation, the oxalic acid concentration is higher than that of fumaric acid, suggesting that other intermediates exist that directly decompose into oxalic acid. In addition, oxalic acid is not easily oxidized, and its slow degradation rate is another reason for its high concentration in solution. On Mp-SnO_2/BDD and BDD, the c_{max} values of fumaric acid are 3.2 and 4.6 mg L^{-1}, respectively, while the values of oxalic acid are 8.6 and 12.0 mg L^{-1}, respectively. This indicates that Mp-SnO_2/BDD also has a better degradation ability for carboxylic acid intermediates. In addition, dehalogenation is an important process during the degradation of halogenated organic pollutants, so the release of free Cl^- during CA degradation also was studied. As shown in Fig. S6, the evolution of Cl^- has the same tendency on Mp-SnO_2/BDD and BDD, that is, it continually accumulates to reach a maximum value and then slowly decrease. The Cl^- concentration reaches a maximum of 9.9 mg L^{-1} at 120 min on Mp-SnO_2/BDD, while the Cl^- concentration is up to 12.9 mg L^{-1} at 150 min on BDD. It indicates that C-Cl bonds in the CA molecules are more easily attacked by ·OH generated on Mp-SnO_2/BDD, consequently the Cl^- concentration reaches a maximum in a shorter time. In contrast, the Cl^- concentration increases all the time with traditional SnO_2/Ti until the degradation finished. Provided that the chloride atoms are all converted to Cl^- exclusively, the maximum theoretical concentration of Cl^- is about 33.1 mg L^{-1} for the 200 mg L^{-1} CA wastewater. However, it was found that the concentrations of chloride ion in all cases are lower than the theoretical value. Based on the results, it is speculated that some of released Cl^- may be further oxidized to generate Cl_2, and others may be involved in side reactions or formed complexes besides existing as free Cl^-. Therefore, the detected Cl^- concentration starts to decrease after reaching a maximum on BDD and Mp-SnO_2/BDD. For SnO_2/Ti, the continuous rising of Cl- reflects that chlorine-containing intermediates are not yet dechlorinated completely after 240 min.

Based on the identified intermediates, a plausible CA degradation scheme, including several oxidation pathways on Mp-SnO_2/BDD, is proposed in Fig. 6. The ·OH attack is suggested to occur at three different reaction sites on CA to yield the different primary intermediates (pathways 1–3). Provided that selecting the ring-opening of the benzene ring as a demarcation point, the degradation reaction can be divided into two major steps. The first step is the formation of various aromatic intermediates when the parent pollutant is attacked by oxidative, free radicals without a ring-opening, and the decomposition into a carboxylic acid is the second step. In terms of the inactive Mp-SnO_2/BDD, the degradation of organic pollutants in an aqueous solution is mainly triggered by the ·OH adsorbed on the electrode surface and the free ·OH with a strong oxidizing ability distributed in the double layer zone, which can promote the mineralization via a series of processes including hydroxylation, hydrogenation, and bond cleavage [43,44]. In route 1, the No. 1 carbon site of CA is attacked by ·OH, and the C–O bond is broken, generating 4-chlorophenol after the loss of 2-hydroxyisobutyric acid. Then, the dechlorination of *p*-chlorophenol occurs to produce hydroquinone, which is further oxidized to p-benzoquinone [30]. In route 2, dechlorination is directly achieved by ·OH attacking the Cl-linked carbon atom and it is followed by the release of 2-hydroxyisobutyric acid, leading to the production of p-benzoquinone. In route 3, the No. 2 carbon atom on the benzene ring is attacked, and 1,2,4-benzenetriol is generated via multiple hydroxylation reactions. Subsequently, benzoquinone and 1,2,4-benzenetriol are continuously degraded by ·OH to form various small carboxylic acids, such as fumaric acid, maleic acid, oxalic acid, formic acid and other small substances with a low toxicity, via cleavage of the benzenic ring, and this

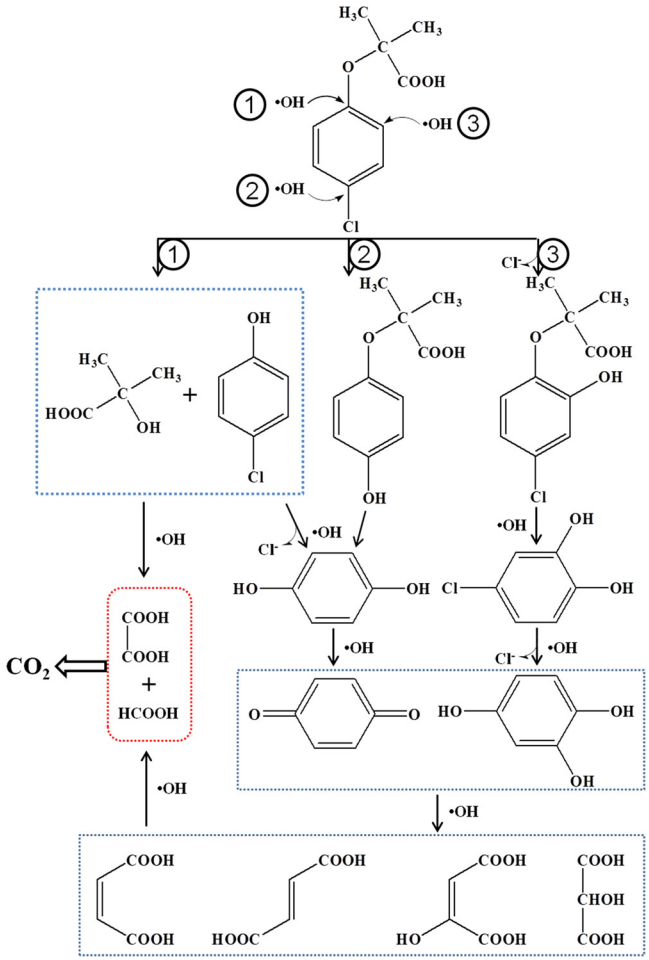

Fig. 6. Possible decomposition pathways for the total mineralization of CA with Mp-SnO_2/BDD.

degradation continues until the acids are completely mineralized to CO_2 and H_2O [45]. The electrocatalytic oxidation of CA by ·OH is very complicated, and the detected by-products are only a limited portion in the degraded solution samples. In short, CA can be rapidly decomposed and mineralized by electrochemical oxidation on Mp-SnO_2/BDD under mild conditions, and the process has many advantages over that on BDD, including a better electrocatalytic performance, higher mineralization current efficiency, and lower energy consumption.

To further clarify the electrocatalytic oxidation process, CV curves for five cycles were obtained in a 0.05 M Na_2SO_4 + 200 mg L^{-1} CA solution for Mp-SnO_2/BDD, BDD, and SnO_2/Ti. As shown in Fig. 3B and Fig. S7, 8, the direct electrocatalytic oxidation of CA occurs even at 1.2–1.3 V on the three electrodes; however, the oxidation peak potentials are different in the first scan cycle, i.e., Mp-SnO_2/BDD (1.50 V) < SnO_2 (1.65 V) < BDD (2.0 V), implying that CA is more easily oxidized on Mp-SnO_2/BDD. During the CV test, the high potentials were all controlled below their corresponding OEP at each electrode. In that potential region, the electrocatalysis of CA is mainly dominated by the direct electrocatalytic oxidation that occurs on the electrode surface. Thus, the decrease in the oxidation peak current may be due to passivation caused by electro-polymerization as the number of scanning cycles increases. The oxidation peak in the fifth scanning cycle for Mp-SnO_2/BDD is more apparent than that for the other two electrodes, which indicates that Mp-SnO_2/BDD has a better anti-passivation capability.

The anodic electrochemical degradation of organic pollutants is mainly initiated by indirect electrocatalytic oxidation at a high applied potential (i.e., higher than the OEP). Therefore, to compare the indirect electrocatalytic oxidation ability of Mp-SnO_2/BDD and BDD, 0.05 M Na_2SO_4 and 0.05 M Na_2SO_4 + 200 mg L^{-1} CA test solutions were used to measure the change in the current over time at 1 V and 4 V (vs. SCE), respectively. Fig. 3C shows that the current density increases from 5.9 for BDD to 7.1 mA cm^{-1} for Mp-SnO_2/BDD in the blank solution at 4 V, which demonstrates again that the electrical conductivity is enhanced for Mp-SnO_2/BDD. Moreover, no evident change in the current density is observed on two electrodes at 1 V in the presence of CA because the applied potential is lower than the oxidation potential of CA. The current densities on BDD and Mp-SnO_2/BDD are both enhanced at 4 V with the addition of CA, and the value of Mp-SnO_2/BDD reaches 7.8 mA cm^{-2}. The difference in the current densities with or without CA is 0.2 mA cm^{-2} on BDD, which is an amplitude increase 2.9% less than that on Mp-SnO_2/BDD (9.8%) and can be ascribed to the faradic current generated from the electrocatalytic oxidation of CA. The result reveals that the modification with SnO_2 improved the electrocatalytic performance of BDD, and organic pollutants can quickly diffuse and be oxidized in the vicinity of Mp-SnO_2/BDD. In addition, the electron transfer rate at the electrode interface is significantly enhanced. It is speculated that the improvement in the electrocatalytic performance is related to the 2D, macroporous microstructure and the chemical properties of the active electrocatalyst, which can provide a large number of electrocatalytic sites for the rapid degradation of organic pollutants.

Taking actual application into account, the stability of anode is also our concern. The reusability of Mp-SnO_2/BDD was investigated with repetitious CA degradation tests. The result indicates that removal of CA and COD with the Mp-SnO_2/BDD decreased little, which remains all above 90% for CA and 85% for COD removals after five consecutive runs. To evaluate structural stability, the morphology of the used Mp-SnO_2/BDD was examined by SEM. Compared with the SEM image of as-prepared one in Fig. 2B, it is found that the well-defined 2D macroporous structure of SnO_2 is also maintained (Fig. S9), demonstrating that the Mp-SnO_2/BDD is stable and robust.

4. Conclusions

In summary, we developed a facile approach to fabricate Mp-SnO_2/BDD and studied its electrochemical degradation for recalcitrant CA. Due to bifunctional interface, the Mp-SnO_2/BDD simultaneously possesses both the excellent electrocatalytic activity of SnO_2 and high OEP of BDD. CA removal is reached 95% min and COD removal is 90% after 240 with Mp-SnO_2/BDD, while the value is respectively 83% and 75% using BDD. The degradation of CA fits to the pseudo-first-order kinetics. The enhanced degradation and mineralization ability is directly related to improved electrochemical properties. In addition, several main aromatic intermediate products including 4-chlorophenol, hydroquinone, 4-chlorocatechol, p-benzoquinone and 1,2,4-benzenetriol were detected in the early stage, and some small molecular carboxylic acids such as maleic acid, fumaric acid, oxalic acid and formic acid were identified subsequently. The possible CA decomposition pathways is also proposed. The monolayer hard template method is scalable to construct other 2D macroporous electrodes, and Mp-SnO_2/BDD would be an efficient and promising electrode material for wastewater remediation.

Acknowledgments

This work was financially supported by the National Natural Science Foundation of China (Nos. 21537003, 21507103), the Natural Science Basic Research Plan in Shaanxi Province of China (No. 2016JQ5048), and the Scientific Research Program Funded by the Shaanxi Provincial Education Department (No. 15JK1383).

Appendix A. Supplementary data

Supplementary material related to this article can be found, in the

online version, at doi:https://doi.org/10.1016/j.apcatb.2018.06.023.

References

[1] K.R. Zodrow, Q. Li, R.M. Buono, W. Chen, G. Daigger, L. Duenas-Osorio, M. Elimelech, X. Huang, G. Jiang, J.-H. Kim, B.E. Logan, D.L. Sedlak, P. Westerhoff, P.J.J. Alvarez, Environ. Sci. Technol. 51 (2017) 10274–10281.
[2] Y.-U. Shin, H.-Y. Yoo, S. Kim, K.-M. Chung, Y.-G. Park, K.-H. Hwang, S.W. Hong, H. Park, K. Cho, J. Lee, Environ. Sci. Technol. 51 (2017) 10700–10710.
[3] J.T. Jasper, O.S. Shafaat, M.R. Hoffmann, Environ. Sci. Technol. 50 (2016) 10198–10208.
[4] A. Fernandes, M.J. Pacheco, L. Ciriaco, A. Lopes, Appl. Catal. B: Environ. 176 (2015) 183–200.
[5] E. Brillas, C.A. Martinez-Huitle, Appl. Catal. B: Environ. 166 (2015) 603–643.
[6] Y. Yang, J. Shin, J.T. Jasper, M.R. Hoffmann, Environ. Sci. Technol. 50 (2016) 8780–8787.
[7] N. Flores, P. Lluis Cabot, F. Centellas, J. Antonio Garrido, R. Maria Rodriguez, E. Brillas, I. Sires, J. Hazard. Mater. 321 (2017) 566–575.
[8] E. Brillas, I. Sires, M.A. Oturan, Chem. Rev. 109 (2009) 6570–6631.
[9] N. Yang, J.S. Foord, X. Jiang, Carbon 99 (2016) 90–110.
[10] G. Sine, I. Duo, B. El Roustom, G. Foti, C. Comninellis, J. Appl. Electrochem. 36 (2006) 847–862.
[11] M. Limat, B. El Roustom, H. Jotterand, G. Foti, C. Comninellis, Electrochim. Acta 54 (2009) 2410–2416.
[12] Y. Zhang, V. Suryanarayanan, I. Nakazawa, S. Yoshihara, T. Shirakashi, Electrochim. Acta 49 (2004) 5235–5240.
[13] X.L. Tong, G.H. Zhao, M.C. Liu, T.C. Cao, L. Liu, P.Q. Li, J. Phys. Chem. C 113 (2009) 13787–13792.
[14] H. Lin, J. Niu, J. Xu, H. Huang, D. Li, Z. Yue, C. Feng, Environ. Sci. Technol. 47 (2013) 13039–13046.
[15] Z.Y. Zhou, N. Tian, J.T. Li, I. Broadwell, S.G. Sun, Chem. Soc. Rev. 40 (2011) 4167–4185.
[16] B.P. Chaplin, Environ. Sci. Proc. Impacts 16 (2014) 1182–1203.
[17] X.M. Chen, P.D. Yao, D.H. Wang, X.Z. Wu, Chem. Eng. J. 147 (2009) 412–415.
[18] G. Zhao, X. Cui, M. Liu, P. Li, Y. Zhang, T. Cao, H. Li, Y. Lei, L. Liu, D. Li, Environ. Sci. Technol. 43 (2009) 1480–1486.
[19] X.W. Liu, W.W. Li, H.Q. Yu, Chem. Soc. Rev. 43 (2014) 7718–7745.
[20] X.M. Chen, F.R. Gao, G.H. Chen, J. Appl. Electrochem. 35 (2005) 185–191.
[21] M. Panizza, G. Cerisola, Chem. Rev. 109 (2009) 6541–6569.
[22] C. Lopez, Adv. Mater. 15 (2003) 1679–1704.
[23] J.X. Wang, Y.Z. Zhang, S.T. Wang, Y.L. Song, L. Jiang, Acc. Chem. Res. 44 (2011) 405–415.
[24] A. Ziylan, N.H. Ince, J. Hazard. Mater. 187 (2011) 24–36.
[25] R.K. Singh, L. Philip, S. Ramanujam, Water Res. 121 (2017) 20–36.
[26] C. Ridruejo, C. Salazar, P.L. Cabot, F. Centellas, E. Brillas, I. Sires, Chem. Eng. J. 326 (2017) 811–819.
[27] S. Chai, G. Zhao, Y.-n. Zhang, Y. Wang, F. Nong, M. Li, D. Li, Environ. Sci. Technol. 46 (2012) 10182–10190.
[28] J. Sun, C.J. Tang, P. Zhan, Z.L. Han, Z.S. Cao, Z.L. Wang, Langmuir 26 (2010) 7859–7864.
[29] M. Panizza, P.A. Michaud, G. Cerisola, C. Comninellis, J. Electroanal. Chem. 507 (2001) 206–214.
[30] B. Boye, E. Brillas, B. Marselli, P.A. Michaud, C. Comninellis, G. Farnia, G. Sandona, Electrochim. Acta 51 (2006) 2872–2880.
[31] M. Panizza, P.A. Michaud, G. Cerisola, C. Comninellis, Electrochem. Commun. 3 (2001) 336–339.
[32] Y. Chen, F. Sun, Z. Huang, H. Chen, Z. Zhuang, Z. Pan, J. Long, F. Gu, Appl. Catal. B: Environ. 215 (2017) 8–17.
[33] C. Terashima, K. Arihara, S. Okazaki, T. Shichi, D.A. Tryk, T. Shirafuji, N. Saito, O. Takai, A. Fujishima, ACS Appl. Mater. Interfaces 3 (2011) 177–182.
[34] B. Grzeta, E. Tkalcec, C. Goebbert, M. Takeda, M. Takahashi, K. Nomura, M. Jaksic, J. Phys. Chem. Solids 63 (2002) 765–772.
[35] S.Y. Yang, Y.S. Choo, S. Kim, S.K. Lim, J. Lee, H. Park, Appl. Catal. B: Environ. 111 (2012) 317–325.
[36] Q. Zhang, H. Xu, W. Yan, Electrochim. Acta 61 (2012) 64–72.
[37] X.P. Zhu, M.P. Tong, S.Y. Shi, H.Z. Zhao, J.R. Ni, Environ. Sci. Technol. 42 (2008) 4914–4920.
[38] R. Salgado, A. Oehmen, G. Carvalho, J.P. Noronha, M.A.M. Reis, J. Hazard. Mater. 241–242 (2012) 182–189.
[39] W.Z. Li, Y. Ding, Q. Sui, S.G. Lu, Z.F. Qiu, K.F. Lin, Front. Environ. Sci. Eng. 6 (2012) 445–454.
[40] M. Kuster, M.J. de Alda, M.D. Hernando, M. Petrovic, J. Martin-Alonso, D. Barcelo, J. Hydrol. 358 (2008) 112–123.
[41] J. Martin, D. Camacho-Munoz, J.L. Santos, I. Aparicio, E. Alonso, J. Environ. Monit. 13 (2011) 2042–2049.
[42] I. Sires, P.L. Cabot, F. Centellas, J.A. Garrido, R.M. Rodriguez, C. Arias, E. Brillas, Electrochim. Acta 52 (2006) 75–85.
[43] S. Chai, Y. Wang, Y.-n. Zhang, M. Liu, Y. Wang, G. Zhao, Environ. Sci. Technol. 51 (2017) 8067–8076.
[44] B. Marselli, J. Garcia-Gomez, P.A. Michaud, M.A. Rodrigo, C. Comninellis, J. Electrochem. Soc. 150 (2003) D79–D83.
[45] I. Sires, F. Centellas, J.A. Garrido, R.M. Rodriguez, C. Arias, P.L. Cabot, E. Brillas, Appl. Catal. B: Environ. 72 (2007) 373–381.